Published in final edited form as:
Bioconjug Chem. 2010 July 21; 21(7): 1297–1304. doi:10.1021/bc1000998.

Optical Imaging of Bacterial Infection in Living Mice Using Deep-Red Fluorescent Squaraine Rotaxane Probes

Alexander G. White, **Na Fu**, **W. Matthew Leevy**, **Jung-Jae Lee**, **Michael A. Blasco**, and **Bradley D. Smith***
Department of Chemistry and Biochemistry and the Notre Dame Integrated Imaging Facility, 236 Nieuwland Science Hall, University of Notre Dame, Notre Dame, IN 46556, USA

Abstract

Two structurally related fluorescent imaging probes allow optical imaging of bacterial leg infection models in living athymic and immunocompetent mice. Structurally, the probes are comprised of a deep-red fluorescent squaraine rotaxane scaffold with two appended bis(zinc(II)-dicolylamine) (bis(Zn-DPA)) targeting ligands. The bis(Zn-DPA) ligands have high affinity for the anionic phospholipids and related biomolecules that reside within the bacterial envelope, and they are known to selectively target bacterial cells over the nearly uncharged membrane surfaces of healthy mammalian cells. Planar, whole-animal optical imaging studies showed that intravenous dosing of either probe (10 nmol) allowed imaging of localized infections of Gram-positive *Staphylococcus aureus* and Gram-negative *Salmonella enterica* serovar typhimurium. High selectivity for the infected target leg (T) over the contralateral non-target leg (NT) was reflected by T/NT ratios up to six. The infection imaging signal was independent of mouse humoral immune status, and there was essentially no targeting at a site of sterile inflammation induced by injection of λ-carrageenan. Furthermore, the fluorescent probe imaging signal colocalized with the bioluminescence signal from a genetically engineered strain of *S. enterica* serovar typhimurium. Although not highly sensitive (the localized infection must contain at least ~10^6 colony forming units for fluorescence visualization) the probes are remarkably selective for bacterial cells considering their low molecular weight (<1.5 kDa) and simple structural design. The more hydrophilic of the two probes produced a higher T/NT ratio in the early stages of the imaging experiment and washed out more rapidly from the blood clearance organs (liver, kidney). Therefore, it is best suited for longitudinal studies that require repeated dosing and imaging of the same animal. The results indicate that fluorescent probes based on squaraine rotaxanes should be broadly useful for in vivo animal imaging studies, and they further validate the ability of imaging probes with bis(Zn-DPA) ligands to selectively target bacterial infections in living animals.

INTRODUCTION

Optical imaging continues to undergo major advances that produce landmark contributions to biomedical science (1–4). Concurrent with technical improvements in the design and operation of fluorescence microscopes and whole-animal imaging stations, there is an ongoing effort to develop new types of fluorescent molecular probes (5,6). Organic fluorophores are the most common components in the bioimaging probe toolbox, however, they are well known for performance drawbacks like photobleaching, self-quenching, and chemical decomposition (7). These problems are especially prevalent with organic probes

*smith.115@nd.edu, ph: +1 (574) 631 8632, fax: +1 (574) 631 6652.

Supporting Information Available: movie in .avi format showing the real-time change in imaging pixel intensity over three hours for a nude athymic mouse infected with *S. aureus* and treated with probe **1**. This material is available free of charge via the Internet at http://pubs.acs.org.

with excitation/emission wavelengths in the deep-red and near-infrared; a wavelength region that is preferred for biological imaging because there is maximal light penetration through skin and tissue with minimal scattering (8). Of the few available deep-red and near-infrared fluorophores, the most popular are the carbocyanine dyes (9). In addition to the photochemical drawbacks listed above, the photophysical properties of long-wavelength carbocyanine dyes are known to vary with solvent polarity and the presence of blood serum proteins (10). Together, these problems make it difficult to develop methods for quantitative whole-animal optical imaging. The need for new families of deep-red and near-infrared organic fluorophores is reflected by the ongoing international effort to prepare and evaluate new structural classes (11).

Our research group has invented a novel family of deep-red fluorescent dyes called squaraine rotaxanes (12–20). Squaraines were discovered almost fifty years ago and they exhibit narrow and intense absorption/emission bands. Squaraine dyes and their conjugates have been prepared and evaluated for various types of in vitro imaging applications (21–23), however, to the best of our knowledge they have never been reported for in vivo imaging in living animals. The most likely reason for this absence is their inherent chemical reactivity. The central squaraine ring is electrophilic and susceptible to attack by biological nucleophiles, thus unprotected squaraine dyes are susceptible to decomposition during in vivo imaging. Squaraine rotaxanes circumvent this stability problem by encapsulating the squaraine fluorophore inside a protective macrocycle. We have demonstrated that squaraine rotaxanes are chemically and photochemically stable and very useful for many types of in vitro cell culture imaging applications (12–20). Two examples are the squaraine rotaxane probes **1** (19) and **2** (24) in Figure 1. They both contain the same squaraine fluorophore with conjugated bis(zinc(II)-dicolylamine) (bis(Zn-DPA)) targeting ligands at each end. The bis(Zn-DPA) ligands have high affinity for anionic cell membranes and they are known to selectively target bacterial cells over the nearly uncharged membrane surfaces of healthy mammalian cells (19,25–27). The bis(Zn-DPA) ligands associate with the anionic phospholipids and related amphiphilic structures that reside within the bacterial envelope (28,29). Preliminary fluorescence microscopy studies of probes **1** and **2** have shown that they stain both Gram-positive and Gram-negative bacteria without inducing an antibiotic effect. The probes are extremely photostable and permit real-time imaging studies of live cell process like bacterial fission. The difference between probes **1** and **2** is the structure of the surrounding macrocycle. The macrocycle in probe **1** has two phenylene units that hardly effect the photophysical properties of the encapsulated squaraine fluorophore, such that probe **1** exhibits excitation/emission wavelengths of 653/675 nm that match the common Cy5 filter set on microscopes and imaging stations. The macrocycle in probe **2** has two anthrylene units that lead to red-shifted excitation/emission of 664/709 nm that match the Cy5.5 filter set.

In this current study, we report that probes **1** and **2** can be used to optically image bacterial infection and that they do not respond to sterile inflammation in living mice. We find that the more hydrophilic probe **1** produces a higher ratio of target to non-target signals in the early stages of the imaging experiment, and appears to be the better infection imaging probe for longitudinal studies that require rapid probe wash out and repeated imaging of the same animal. Our results indicate that fluorescent probes based on squaraine rotaxanes should be broadly useful for in vivo animal imaging studies, and they further validate the ability of imaging probes with bis(Zn-DPA) ligands to selectively target bacterial infections in living animals.

EXPERIMENTAL PROCEDURES

Materials

The probes **1** (5 μM in water, ex: 653 nm, em: 675 nm, log ε 5.1, quantum yield 0.20 in water) and 2 (5 μin water, ex: 664 nm, em: 709 nm, log ε 5.3, quantum yield 0.22) were prepared as previously reported (19,24). These previous reports also include the excitation and emission spectra. Luria-Bertani (LB) broth purchased from BD Medical Supplies (Sparks, MD). Kanamycin, λ-carrageenan, and ATP were purchased from Sigma (St. Louis, MO). Isoflurane was purchased from Butler Animal Health Supply (Dublin, OH). Animals were purchased from Taconic Farms, Inc. (Hudson, NY). *Salmonella enterica* serovar typhimurium FL6 and AM3 were gifts from the laboratory of Professor David Piwnica-Worms (Washington University, School of Medicine, St. Louis, MO) (30).

In vitro Fluorescence Microscopy

Fluorescence microscopy was conducted on a Nikon Eclipse TE-2000 U epifluorescence microscope equipped with Cy5 (Exciter: HQ620/60X, Dichroic: 660LP, Emitter: HQ700/75m) filter. Images were acquired using Metamorph software (v6.2 Molecular Devices, Sunnyvale, CA) and a Photometrics 512 B black & white digital camera (1500×) at 100 ms acquisition time. The data was processed with ImageJ v1.42q software (available for free download at http://rsb.info.nih.gov/ij) as previously described (26).

In vitro Cell Staining

S. enterica serovar typhimurium AM3 was cultured in LB broth containing 30 μg/mL kanamycin after transfer from a preserved agar plate stored at 4 °C. *Staphylococcus aureus* NRS11, *Escherichia coli* K12, *Escherichia coli* UTI89, *Klebsiella pneumoniae* (ATCC #33495), *Proteus vulgaris* (ATCC #49132), and *Pseudomonas aeruginosa* (ATCC #27853) were cultured in LB broth containing no antibiotic after transfer from a preserved agar plate stored at 4 °C. Cells were allowed to grow overnight by incubating at 37 °C and a shaker speed of 200 rpm. *Salmonella* cells were centrifuged at 10000 rpm for 5 min while all other bacterial strains were centrifuged at 5000 rpm for 5 min. Growth media was removed and the cells resuspended in 5 mM TES buffer (145 mM NaCl buffer, pH 7.4). Separate samples of 10^8 colony forming units (CFU) were treated with 10 nmol of probe **1** or **2** and the mixture was incubated in the dark for 15 min at room temperature. After centrifugation at the above speeds for 5 min, the media was discarded and the pellet resuspended in 5 mM TES buffer with vortexing. The stained cells were rinsed with TES buffer by repeating the centrifugation/resuspension cycle.

ATP inhibition of cell staining by probe **1** was performed by adding specific volumes of ATP from a stock solution prior to incubating bacteria and probe for 15 minutes. Region-of-interest (ROI) analysis using ImageJ software produced average pixel intensity for an individual cell. The fluorescence intensities in the bottom of Figure 3 are the average of twenty random bacterial cells in each staining sample.

Minimum inhibitory concentration for probes **1** and **2** against the Gram-positive *S. aureus* NRS11 and Gram-negative *E. coli* UTI89 were determined using a previously described procedure (28).

Animal Preparation

All animal care and procedures were approved by the Notre Dame Institutional Advisory Committee of Animal Care. All animals were anesthetized using 2–3% v/v isoflurane before infection, probe injection, and imaging. Anesthesia during imaging was maintained at 1.5–2% v/v isoflurane. Athymic nude mice (strain NCr Foxn1^{nu}) required no additional

preparation before imaging. Immunocompetent mice (strain ICr) were anesthetized and hair was removed from the lower quarter of the body by clippers followed by depilatory cream.

In vivo Leg Infection/Inflammation Model

An aliquot of *Staphylococcus aureus* NRS11 (~10^8 CFU) in 50 μL of LB growth media was injected into the muscles that overlay the tibia bone in a posterior leg of an athymic or immunocompetent mouse. This anatomical location is not the thigh, which is closer to the body of the mouse. The same location on the contralateral leg was injected with 50 μL of LB media as a vehicle control. For inflammation response, immunocompetent ICr mice were injected with 50 μL of 1 % λ-carrageenan solution into the left posterior leg muscle and injected with 50 μL of a sterile saline solution in the right posterior leg muscle. The mice were then allowed to recover for 6 h before intravenous injection with fluorescent probe via the tail vein. A complete probe toxicity study was not conducted but both the athymic and immunocompetent mice easily tolerated the single doses (10 nmol) of probes **1** or **2** as judged by their continued grooming and nesting activities.

In vivo Fluorescence Planar Imaging

Fluorescence dorsal images were acquired using a Xenogen IVIS Lumina (Caliper Life Sciences, Alameda, CA) for 5 s (Ex 640 ± 25, Em 732 ± 37 nm, binning 2 × 2, f/stop 2, field-of-view 125 mm). IVIS Lumina imaging was controlled by Living Image software (version 3.0) and employed 16-bit TIFF format files. Fluorescence ventral images were acquired using a Kodak Multispectral In Vivo Imaging System FX Pro (Carestream Health, New Haven, CT) for 30 s (Ex 630 ± 10 nm, Em 700 ± 17.5 nm, no binning, f/stop 2.51, focal plane 11.2 mm, Field-of-view 160 mm). Kodak multispectral imaging was controlled by Carestream Molecular Imaging Software (v. 5.0.2.30). Image files were saved as BIP format and converted to 16-bit TIFF format. X-ray acquisition used a 120 s exposure (no binning, f/stop 2.5, focal plane 12.31 mm, Field-of-view 160 mm).

S. enterica serovar typhimurium FL6 is a genetically engineered strain with the *lux*CDABE genes from *Photorhabdus luminescens* which expresses bacterial luciferase and the enzymes for production of its substrate, decanal. The cells continuously emit light and in vivo bioluminescence images were acquired for 3 min (open filter, 16 × 16 binning, f/stop 2.51, Field-of-view 160 mm).

In vivo Image Processing

The 16-bit TIFF images were sequentially opened using the ImageJ software and then converted to an image stack using the “convert images to stack” software command. The stack of images was background subtracted using the rolling ball algorithm (radius 500 pixels). Next, the image stack was set to the “Fire” fluorescence intensity scale (under “Lookup Tables” menu) which color-codes the fluorescence counts contained in each pixel. The stack of images was converted into a montage using the “convert stack to montage” command. A calibration bar was added to the montage using the “calibration bar” command, and the resulting RGB image saved as a TIFF file. ROI analysis was performed by selecting a free-hand ROI from the ImageJ tool bar, and circling the appropriate anatomical location of each mouse. The average pixel intensity of the target (T), non-target (NT), and whole animal was measured and statistical analysis of the cohort produced an average ratio for T/NT with a standard error of the mean.

Biodistribution analysis

After imaging studies, the mice were anesthetized by isoflurane inhalation (2–3%) and euthanized by cervical dislocation. The major organs were dissected, placed on low

reflectance paper, and imaged as described above. The biodistribution image was analyzed in ImageJ by first subtracting the background using the rolling ball method (radius 500 pixels). Free-hand ROIs were drawn around each organ and average intensity values were measured. Statistical analysis of the cohort produced an average pixel intensity relative to the uninfected leg for each organ with a standard error of the mean. Each excised organ attenuates probe signal intensity to a slightly different degree, depending on tissue thickness and pigmentation. Therefore, the biodistribution analysis focused on a comparison of the average intensities for probe **1** and **2** in each organ and assumed that they suffer equal amounts of signal attenuation.

RESULTS

In Vitro Studies

The generality of probe targeting for various bacterial genera was tested by conducting in vitro microscopy experiments using probe **1** and cultures of planktonic *S. aureus*, *E. coli*, *S. enterica* serovar typhimurium AM3, *P. aeruginosa*, *K. pneumoniae*, and *P. vulgaris*. In each case, separate samples of ~10^8 CFU were treated for fifteen minutes with probe **1** (10 μM) in TES, a non phosphate buffer which does not inhibit probe binding to the bacteria. After probe treatment, the bacterial cells were rinsed twice to ensure high contrast microscopy images. As expected, strong fluorescence staining of all genera was observed, although staining of the Gram-negative strains was typically less intense, indicating some steric protection by the second, outer membrane. Shown in Figure 2 are typical images obtained with Gram-positive *S. aureus* NRS11 and Gram-negative *S. enterica* serovar typhimurium AM3 using a standard, deep-red Cy5 filter set. In agreement with previous studies of fluorescent bis(Zn-DPA) probes, the fluorescence emission is localized in the bacterial envelope. Each image shows examples of bacterial cells captured in the process of cell division with bright fluorescence indicating a septum across circular *S. aureus* and a pinched equator for dividing *Salmonella*.

Bis(Zn-DPA) probes are well-known to associate with polyphosphorylated biomolecules and anionic vesicle membranes (31), and the most likely explanation for bacterial staining is coordination of the zinc(II) cations with the phospholipids and phosphorylated amphiphiles in the bacterial envelope. The structural complexity and multifarious components of the bacterial envelope makes it quite challenging to unambiguously prove the cell association mechanism. Imaging studies using the apo-ligands (that is, probe **1** or **2** without the zinc(II) cations) are not possible since they are not soluble in water. Indirect evidence that the bacterial staining is due to association of the bis(Zn-DPA) units with phosphorylated sites in the bacterial envelope was gained by conducting staining inhibition studies with probe **1**. The triphosphate unit in ATP is known to have a strong affinity for bis(Zn-DPA) ligands (32), and as shown in Figure 3, the addition of ATP inhibits, in a dose-dependent manner, the staining of *S. aureus* NRS11 or *E. coli* K12 cells by probe **1**.

Measurements of minimum inhibitory concentrations showed that probes **1** and **2** do not halt the growth of Gram-positive *S. aureus* NRS11 until the probe concentration is 60 μg/mL and they are even less active against Gram-negative *E. coli* UTI89. This agrees with previous studies indicating that imaging probes with bis(Zn-DPA) ligands have a very weak antibiotic effect (27).

Imaging Leg Infection Model in Athymic Mice

Comparison of probes 1 and 2 to image *S. aureus* infection—The in vivo imaging performances of probes **1** and **2** were compared under the same conditions in a leg infection model using two different planar optical imaging stations. Separate cohorts of athymic nude

mice were infected by intramuscular injection of ~10^8 CFU of *S. aureus* NRS11 into the left posterior leg, and as a control the same volume (50 μL) of sterile growth media was injected into the contralateral leg. Six hours after inoculation, the anesthetized mice were given intravenous doses of imaging probes **1** or **2** (10 nmol) and then imaged periodically by illuminating with deep-red light and capturing the resulting fluorescence using a CCD camera. Shown in Figure 4 are typical whole-animal planar fluorescence images (false colored to show average pixel intensity) of two infected mice at 0, 3, and 12 hours after the probe dosage. The probes exhibit quite different pharmacokinetics. With probe **1** the average pixel intensity at the infection site increased rapidly over the first three hours. The appearance was sufficiently fast that it could be followed in real-time while the mouse remained under anesthesia. The supporting information contains a movie showing a typical change in whole-animal fluorescence pixel intensity over the first three hours with probe **1**.

The mouse imaging data was analyzed by region-of-interest (ROI) methods that calculated the ratio of pixel intensities for the infected target leg (T) over the contralateral non-target leg (NT). The intensity scales for different mice cannot be directly compared, however, T/NT ratios account for the differences in intrinsic brightness and allow a comparison of probe signal clearance. At three hours after probe injection, the T/NT ratio for probe **1** was close to six and significantly higher than the value of four for probe **2** (Figure 5a), however, at 21 hours post-injection the T/NT ratio for both probes was about the same. Shown in Figure 5b are plots of the change in average pixel intensity at the infection site and for the whole animal. These plots show that signal contrast at the infection site develops in two different probe-dependent ways. With probe **1** there is a rapid and large absolute increase in pixel intensity at the infection site, with a concomitant slower rate of clearance from the entire animal. With probe **2** there is little intensity change at the infection site, with signal contrast developing because probe clearance from the rest of the animal is faster than from the site of infection.

Imaging bioluminescent *S. enterica* serovar typhimurium infection—The ability of probe **1** to target Gram-negative bacterial infection in athymic mice was evaluated using a bioluminescent strain of *Salmonella*. A cohort of mice were injected with ~10^8 CFU of *S. enterica* serovar typhimurium (strain FL6) in the left leg followed by treatment with 10 nmol of probe **1** via the tail vein six hours later. *S. typhimurium* FL6 is genetically engineered to express bacterial luciferase and its substrate, thus allowing continuous light production. The goal was to determine how much the bacterial bioluminescence colocalized with the fluorescence signal from probe **1**. Shown in Figures 6A and 6B are overlaid images of the planar X-ray with the bioluminescence and fluorescence emissions, respectively. The images were acquired three hours after animal dosing with probe **1**, which in turn was delivered six hours after infection. The bioluminescent signal is quite diffuse and indicates some migration of the bacteria away from the initial injection site. As shown in Figure 6C, which is an overlay of panels A and B, there is a considerable colocalization of the bioluminescence and fluorescence signals. As expected, there is also a strong fluorescence signal from the liver which is a major pathway for probe **1** clearance from the animal. Imaging did not continue beyond the three hour time point because the *Salmonella* bacteria were quite virulent and the mice were euthanized.

Imaging Leg Infection in Immunocompetent Mice

Comparison of probes 1 and 2 to image *S. aureus* infection—Separate cohorts of immunocompetent mice were inoculated by injection of *S. aureus* NRS11 (~10^8 CFU) into the left posterior leg and an equal volume (50 μL) of sterile growth media was injected as a control into the contralateral leg. Six hours later, the mice were given intravenous doses of imaging probes **1** or **2** (10 nmol). Shown in Figure 7 are whole-animal images of an infected

mouse at 0, 3, and 12 hours after the probe dosage. The imaging montages are quite similar to that obtained with the athymic mice. As shown in Figure 8, the T/NT ratio with probe **1** reached a maximum of six, and then returned to a value of four, whereas the T/NT ratio with probe **2** steadily rose to the same final value over the 21 h period. Compared to immunocompetent mice, athymic mice have an attenuated humoral immune system, however, both mice strains have innate immunity which is the predominant host defense within the timeframe of the experiment. This explains why there was no measurable difference between in vivo T/NT ratios (compare Figures 5 and 8).

After in vivo imaging was complete, the mice were euthanized and the excised organs were imaged to establish probe biodistribution. Shown in Figure 9 is a comparison of the probe fluorescence (average pixel intensity) from each organ, relative to the uninfected leg muscle which was set to a value of one. The bar graph shows that probe **2** was retained more strongly in all organs than the more hydrophilic probe **1**. There was more of probe **2** in the excised infected leg muscle than probe **1**, even though the in vivo T/NT ratios at the time-point immediately before sacrifice were essentially equal. This suggests that more of probe **1** partitions into the extracellular fluid that surrounds the infection site and that this fluid is lost upon necropsy.

The in vivo detection limit using probe **1** for *S. aureus* infection in immunocompetent mice was determined by injecting serially diluted inoculations and keeping the probe dose (10 nmol) constant. Infections generated by injecting 10^6 CFU could be detected using the above whole-animal imaging protocol, whereas injections of 10^5 CFU could not (data not shown).

The ability of probe **1** to localize in a site of sterile inflammation was evaluated using a model of inflammation induced by the seaweed-derived irritant λ-carrageenan (33). Three cohorts of three immunocompetent mice were injected in the left leg with 50 μL doses containing either: (a) ~10^8 CFU of *S. aureus* in LB broth, (b) 1 % λ-carrageenan solution, or (c) saline. Six hours later, each mouse was dosed with 10 nmol of probe **1** via the tail vein, and then imaged periodically over the following 18 hours. The λ-carrageenan induced considerable swelling, as judged by physical observation. But as shown in Figure 10, the imaging signal from this inflammation site was quite small compared to the signal for *S. aureus* infection, although slightly higher than the imaging signal obtained with saline injection.

DISCUSSION

Most of the published whole-animal optical imaging studies of bacterial infection in small animals have employed bioluminescent bacteria and explored questions concerning migration and colonization of the bacteria or they have developed an in vivo model for testing the efficacy of drug candidates (34,35). The value of bioluminescent infection models is undisputed but the method has some limitations. The signal is dependent on local ATP and oxygen levels and thus is not appropriate for bacteria in hypoxic conditions. The technique requires genetically modified bacteria which is often not possible or requires extensive time and biotechnology resources. The development of optical probes that can target all genera of bacterial infection is a complementary technology that can be employed in situations where bioluminescence is not applicable. In addition, there is the possibility of developing the synthetic probes for use in humans. Optical probes should be useful for imaging of shallow-tissue infections or fluorescence guided surgery, and it should be possible to replace the fluorophore with a reporter group that enables deep-tissue imaging. At present, the standard method for deep-tissue imaging of bacterial infection is to look for the associated inflammation response (36), but inflammation is a clinically ambiguous

parameter that can lead to a false positive diagnosis. Despite the efforts of many international imaging groups, several recent review articles have concluded that there is currently no validated bacterial imaging probe that can distinguish infection from sterile inflammation (37–41). Over the past twenty years, various bacterial affinity ligands have been examined including antibiotic drugs (42), antimicrobial peptides (43,44), sugars (45), bacteria-binding peptides (46), antibodies (47), and enzyme substrates (48). While a few radiotracer probes for bacteria have advanced to large-scale human clinical trials, the evidence for clear success is not compelling (36–41). New classes of targeting ligands are needed and synthetic zinc coordination complexes are a promising new lead. The results reported in this study further demonstrate the remarkably selective bacterial targeting capabilities of bis(Zn-DPA) affinity ligands.

The deep-red fluorescent squaraine rotaxane probes **1** or **2** can readily target model leg infections in living mice but at least 10^6 CFU is needed for in vivo optical visualization. The high selectivity for infected target leg over the contralateral non-target leg is reflected by T/NT ratios high as six (Figure 5 and 8), which compares favorably with the results of other infection imaging probes in the literature (49). The bis(Zn-DPA) ligands have a moderate affinity for polyphosphorylated molecules such as pyrophosphate and ATP, which are present in serum at micromolar concentrations (50–52). Nonetheless, the probes are apparently transferred from carrier serum proteins and phosphorylated molecules in the bloodstream/extracellular matrix to phosphorylated sites in the bacterial envelope. Our previous histological analyses of infected leg muscles that have been targeted by bis(Zn-DPA) probes indicate that the probes selectively associate with the bacterial cells (26). Furthermore, we have previously demonstrated that a control dye lacking a bis(Zn-DPA) ligand does not target the infection site (26). This current study provides additional evidence for high bacterial selectivity by showing that the imaging signal from probe **1** closely colocalizes with the bioluminescence signal from genetically engineered *S. enterica* serovar typhimurium (Figure 6) and it does not strongly target a site of sterile inflammation (Figure 10). The ability to distinguish between infection and sterile inflammation is one of the major applications of infection imaging and imaging probes with this selective targeting capability are quite rare and highly coveted.†

Probe **1** is more hydrophilic than probe **2** and this is likely a major reason for the differences in probe clearance rates. The in vivo signal intensity for probe **1** at the infection site increases substantially during the first few hours after probe injection and then washes out, whereas the in vivo signal intensity for probe **2** at the infection site hardly changes over this time period (Figure 5). At the end of the 21 h imaging experiment the in vivo T/NT ratios for probes **1** and **2** are equal (Figures 5 and 8) yet ex vivo analysis of the organs indicates that there is more of probe **2** in the infected leg muscle. Taken together these results suggest that the relatively hydrophilic probe **1** partitions more into the extracellular fluid that surrounds the swollen infection site and because it is closer to the surface of the body there is an increase in fluorescence signal. This explains both the apparent build up of in vivo imaging signal at the infection site over three hours and the partial loss of probe mass from the infected leg muscle after necropsy.

It is worth comparing the in vivo imaging performance of squaraine rotaxane probes **1** and **2** with the performance of our previously reported probe that contained a cyanine dye and a single bis(Zn-DPA) affinity ligand (26). The cyanine probe exhibits near-IR excitation/fluorescence wavelengths of 794/810 nm that are within the optimal window for maximum penetration of light through skin and tissue, however, its brightness can be attenuated by

†As discussed previously (26,27), bis(Zn-DPA) probes preferentially target the small and highly anionic surfaces of bacterial cells in preference to the nearby apoptotic and necrotic host mouse cells whose larger surfaces are also anionic but more diffusely charged.

self-quenching. Although the deep-red absorption/fluorescence wavelengths of probes **1** and **2** have poorer tissue penetration than the cyanine probe, they nonetheless could be employed at almost ten-fold lower concentrations and still produce more intense signals in the same leg infection models. The ability to employ lower probe doses is a major benefit because there is less concern with probe toxicity, both to the animal and also to the bacterial infection. This latter point is especially important if the goal is to develop an infection imaging method for assessing in vivo efficacy of drug candidates (53–55). Clearly this type of application requires that the probe not interfere with the course of the infection. Another advantage with the deep-red fluorescence of probes **1** and **2** is that it can be seen with the naked eye and thus is quite convenient for in vitro microscopy studies. (19) Therefore, the exact same probe can be employed for both in vitro and in vivo imaging studies. Yet another attractive practical feature with probes **1** and **2** is high water solubility, which facilitates formulation and intravenous delivery. A final point is that the different wavelengths of the above three bacterial imaging probes can be readily distinguished by the filter sets and spectral unmixing algorithms on modern microscopes and imaging stations, thus, enabling fluorescence imaging experiments that label and track separate populations of bacteria in the same sample.

CONCLUSIONS

Squaraine rotaxanes are a new family of deep-red fluorophores that exhibit extremely high chemical and photochemical stability. The results of this study show that they can be converted into effective in vivo imaging probes for optical imaging in rodents. The fluorescent imaging probes **1** and **2** contain two bis(Zn-DPA) affinity ligands that allow targeting of localized bacterial infections over healthy host tissue in living mice. Although not highly sensitive (the infection must contain at least ~10^6 CFU for optical visualization) the probes are remarkably selective for bacterial cells considering their low molecular weight (<1.5 kDa) and simple structural design. The in vivo signal contrast from probe **1** is higher than probe **2** and it clears more rapidly from uninfected organs, thus probe **1** is probably the best suited for most types of small animal imaging applications. Regarding possible translation to human medicine, the limited tissue penetration of deep-red light means that these probes can only be employed for shallow-tissue imaging, or infection sites that can be observed using endoscopes. Another possible application is fluorescence-guided surgery, where the surgeon employs the probes in conjunction with suitable imaging technology to identify and completely remove all bacterial cells.

Supplementary Material

Refer to Web version on PubMed Central for supplementary material.

Acknowledgments

This study was supported by the NIH, the University of Notre Dame, the Notre Dame Integrated Imaging Facility, and the Freimann Life Sciences Center. We thank Kelly Flentie and the laboratory of Professor Piwnica-Worms, Washington University, School of Medicine, St. Louis, MO, for the generous gift of *Salmonella* bacteria.

LITERATURE CITED

1. Demchenko, AP. Introduction to Fluorescence Sensing. New York: Springer; 2009.
2. Hilderbrand SA, Weissleder R. Near-infrared fluorescence: application to in vivo molecular imaging. Curr. Opin. Chem. Biol. 2009; 14:71–79. [PubMed: 19879798]
3. Levitt JA, Matthews DR, Ameer-Beg SM, Suhling K. Fluorescence lifetime and polarization-resolved imaging in cell biology. Curr. Opin. Biotechnol. 2009; 20:28–36. [PubMed: 19268568]

4. Tuchin, VV. Tissue optics: light scattering methods and instruments for medical diagnosis. 2nd ed.. Bellingham, Wash: SPIE/International Society for Optical Engineering; 2007.
5. Kobayashi H, Ogawa M, Alford R, Choyke PL, Urano Y. New strategies for fluorescent probe design in medical diagnostic imaging. Chem. Rev. 2010 ASAP, doi: 10.1021/cr900263j.
6. Terai T, Nagano T. Fluorescent probes for bioimaging applications. Curr. Opin. Chem. Biol. 2008; 12:515–521. [PubMed: 18771748]
7. Resch-Genger U, Grabolle M, Cavaliere-Jaricot S, Nitschke R, Nann T. Quantum dots versus organic dyes as fluorescent labels. Nat. Methods. 2008; 5:763–775. [PubMed: 18756197]
8. Licha K. Contrast agents for optical imaging. Top. Curr. Chem. 2002; 222:1–29.
9. Mishra A, Behera RK, Behera PK, Mishra BK, Behera GB. Cyanines during the 1990s: a review. Chem. Rev. 2000; 100:1973–2011. [PubMed: 11749281]
10. Yuan BH, Chen NG, Zhu Q. Emission and absorption properties of indocyanine green in Intralipid solution. J. Biomed. Opt. 2004; 9:497–503. [PubMed: 15189087]
11. Escobedo JO, Rusin O, Lim S, Strongin RM. NIR dyes for bioimaging applications. Curr. Opin. Chem. Biol. 2009; 14:64–70. [PubMed: 19926332]
12. Arunkumar E, Forbes CC, Noll BC, Smith BD. Squaraine-derived rotaxanes: Sterically protected fluorescent near-IR dyes. J. Am. Chem. Soc. 2005; 127:3288–3289. [PubMed: 15755140]
13. Arunkumar E, Fu N, Smith BD. Squaraine-derived rotaxanes: Highly stable, fluorescent near-IR dyes. Chem. Eur. J. 2006; 12:4684–4690.
14. Arunkumar E, Sudeep PK, Kamat PV, Noll BC, Smith BD. Singlet oxygen generation using iodinated squaraine and squaraine-rotaxane dyes. New J. Chem. 2007; 31:677–683.
15. Fu N, Baumes JM, Arunkumar E, Noll BC, Smith BD. Squaraine rotaxanes with boat conformation macrocycles. J. Org. Chem. 2009; 74:6462–6468. [PubMed: 19639940]
16. Fu N, Gassensmith JJ, Smith BD. Effect of stopper size on squaraine rotaxane stability. Supramol. Chem. 2009; 21:118–124. [PubMed: 20376290]
17. Gassensmith JJ, Barr L, Baumes JM, Paek A, Nguyen A, Smith BD. Synthesis and photophysical investigation of squaraine rotaxanes by "clicked capping". Org. Lett. 2008; 10:3343–3346. [PubMed: 18582079]
18. Gassensmith JJ, Baumes JM, Smith BD. Discovery and early development of squaraine rotaxanes. Chem. Commun. 2009; 42:6329–6338.
19. Johnson JR, Fu N, Arunkumar E, Leevy WM, Gammon ST, Piwnica-Worms D, Smith BD. Squaraine rotaxanes: Superior substitutes for Cy-5 in molecular probes for near-infrared fluorescence cell imaging. Angew. Chem. Int. Ed. 2007; 46:5528–5531.
20. Xiao SZ, Fu N, Peckham K, Smith BD. Efficient synthesis of fluorescent squaraine rotaxane dendrimers. Org. Lett. 2010; 12:140–143. [PubMed: 19957971]
21. Jisha VS, Arun KT, Hariharan M, Ramaiah D. Site-selective binding and dual mode recognition of serum albumin by a squaraine dye. J. Am. Chem. Soc. 2006; 128:6024–6025. [PubMed: 16669657]
22. Thomas J, Sherman DB, Amiss TJ, Andaluz SA, Pitner JB. Synthesis and biosensor performance of a near-IR thiol-reactive fluorophore based on benzothiazolium squaraine. Bioconjugate Chem. 2007; 18:1841–1846.
23. Umezawa K, Cittierio D, Suzuki K. Water-soluble NIR fluorescent probes based on squaraine and their application for protein Labeling. Anal. Sci. 2008; 24:213–217. [PubMed: 18270411]
24. Lee JJ, White AG, Baumes JM, Smith BD. Microwave-assisted slipping synthesis of fluorescent squaraine rotaxane probe for bacterial imaging. Chem. Commun. 2010; 46:1068–1069.
25. Leevy WM, Gammon ST, Jiang H, Johnson JR, Maxwell DJ, Jackson EN, Marquez M, Piwnica-Worms D, Smith BD. Optical imaging of bacterial infection in living mice using a fluorescent near-infrared molecular probe. J. Am. Chem. Soc. 2006; 128:16476–16477. [PubMed: 17177377]
26. Leevy WM, Gammon ST, Johnson JR, Lampkins AJ, Jiang H, Marquez M, Piwnica-Worms D, Suckow MA, Smith BD. Noninvasive optical imaging of staphylococcus aureus bacterial infection in living mice using a bis-dipicolylamine-zinc(II) affinity group conjugated to a near-infrared fluorophore. Bioconjugate Chem. 2008; 19:686–692.

27. Leevy WM, Johnson JR, Lakshmi C, Morris J, Marquez M, Smith BD. Selective recognition of bacterial membranes by zinc(II)-coordination complexes. Chem. Commun. 2006; 15:1595–1597.
28. DiVittorio KM, Leevy WM, O'Neil EJ, Johnson JR, Vakulenko S, Morris JD, Rosek KD, Serazin N, Hilkert S, Hurley S, Marquez M, Smith BD. Zinc(II) coordination complexes as membrane-active fluorescent probes and antibiotics. Chembiochem. 2008; 9:286–293. [PubMed: 18076009]
29. Ganesh V, Bodewits K, Bartholdson SJ, Natale D, Campopiano DJ, Mareque-Rivas JC. Effective binding and sensing of lipopolysaccharide: combining complementary pattern recognition receptors. Angew. Chem. Int. Ed. 2009; 48:356–360.
30. Flentie KN, Qi M, Gammon ST, Razia Y, Lui F, Marpegan L, Manglik A, Piwnica-Worms D, McKinney JS. Stably integrated luxCDABE for assessment of Salmonella invasion. Mol. Imaging. 2008; 7:222–233. [PubMed: 19123992]
31. O'Neil EJ, Smith BD. Anion recognition using dimetallic coordination complexes. Coord. Chem. Rev. 2006; 250:3068–3080.
32. Hanshaw RG, Hilkert SM, Hua J, Smith BD. An indicator displacement system for fluorescent detection of phosphate oxyanions under physiological conditions. Tetrahedron Lett. 2004; 45:8721–8724.
33. Yvonne Wan YJ, Badr MZ. Inhibition of carrageenan-induced cutaneous inflammation by PPAR agonists is dependent on hepatocyte-specific retinoid X receptor alpha. PPAR Res. 2006; 2006 Article ID 96341.
34. Hutchens M, Luker GD. Applications of bioluminescence imaging to the study of infectious diseases. Cell. Microbiol. 2007; 9:2315–2322. [PubMed: 17587328]
35. Leevy WM, Serazin N, Smith BD. Optical imaging of bacterial infection models. Drug Discovery Today: Disease Models. 2007; 4:91–97. [PubMed: 20376332]
36. Goldsmith SJ, Vallabhajosula S. Clinically proven radiopharmaceuticals for infection imaging: mechanisms and applications. Sem. Nucl. Med. 2009; 39:2–10.
37. Chianelli M, Boerman OC, Malviya G, Galli F, Oyen WJG, Signore A. Receptor binding ligands to image infection. Curr. Pharm. Des. 2008; 14:3316–3325. [PubMed: 19075710]
38. Gemmel F, Dumarey N, Welling M. Future diagnostic agents. Semin. Nucl. Med. 2009; 39:11–26. [PubMed: 19038597]
39. Oyen WJ, Corstens FH, Boerman OC. Discriminating infection from sterile inflammation: can radiolabelled antibiotics solve the problem? Eur. J. Nucl. Med. Mol. Imaging. 2005; 32:151–152. [PubMed: 15592927]
40. Signore A, D'Alessandria C, Lazzeri E, Dierckx R. Can we produce an image of bacteria with radiopharmaceuticals? Eur. J. Nucl. Med. Mol. Imaging. 2008; 35:1051–1055. [PubMed: 18398606]
41. Welling M, Stokkel M, Balter J, Sarda-Mantel L, Meulemans A, Le Guludec D. The many roads to infection imaging. Eur. J. Nucl. Med. Mol. Imaging. 2008; 35:848–849. [PubMed: 18188558]
42. Britton KE, Wareham DW, Das SS, Solanki KK, Amaral H, Bhatnagar A, Katamihardja AH, Malamitsi J, Moustafa HM, Soroa VE, Sundram FX, Padhy AK. Imaging bacterial infection with (99m)Tc-ciprofloxacin (Infecton). J. Clin. Pathol. 2002; 55:817–823. [PubMed: 12401818]
43. Lupetti A, Welling MM, Pauwels EKJ, Nibbering PH. Radiolabelled antimicrobial peptides for infection detection. Lancet Inf. Dis. 2003; 3:223–229.
44. Saeed M, Iqbal J, Khan MA, Irfanullah J, Jehangir M, Khan B, ul-Haq I, Muhammad MPG, Nadeem MA, Shehzad M, Imran MB. Tc-99m-labeled antimicrobial peptide ubiquicidin (29–41) accumulates less in Escherichia coli infection than in Staphlococcus aureus infection. J. Nucl. Med. 2004; 45:849–856. [PubMed: 15136636]
45. Qu LW, Luo PG, Taylor S, Lin Y, Huang WJ, Anyadike N, Tzeng TRJ, Stutzenberger F, Latour RA, Sun YP. Visualizing adhesion-induced agglutination of Escherichia coli with mannosylated nanoparticles. J. Nanosci. Nanotechnol. 2005; 5:319–322. [PubMed: 15853155]
46. Dhayal B, Henne WA, Doorneweerd DD, Reifenberger RG, Low PS. Detection of Bacillus subtilis spores using peptide-functionalized cantilever arrays. J. Am. Chem. Soc. 2006; 128:3716–3721. [PubMed: 16536545]

47. Zhao XJ, Hilliard LR, Mechery SJ, Wang YP, Bagwe RP, Jin SG, Tan WH. A rapid bioassay for single bacterial cell quantitation using bioconjugated nanoparticles. Proc. Nat. Acad. Sci. U.S.A. 2004; 101:15027–15032.
48. Bettegowda C, Foss CA, Cheong I, Wang Y, Diaz L, Agrawal N, Fox J, Dick J, Dang LH, Zhou S, Kinzler KW, Vogelstein B, Pomper MG. Imaging bacterial infections with radiolabeled 1-(2'-deoxy-2'-fluoro-β-D-arabinofluranosyl)-5-iodouracil. Proc. Nat. Acad. Sci. U.S.A. 2005; 102:1145–1150.
49. Welling MM, Lupetti A, Balter HS, Lanzzeri S, Souto B, Rey AM, Savio EO, Paulusma-Annema A, Pauwels EK, Nibbering PH. 99mTc-labeled antimicrobial peptides for detection of bacterial and Candida albicans infections. J. Nucl. Med. 2001; 42:788–794. [PubMed: 11337578]
50. Gorman MW, Feigl EO, Buffington CW. Human plasma ATP concentration. Clin. Chem. 2007; 53:318–325. [PubMed: 17185366]
51. Preston CJ, Noorwali A, Challa A, Paterson AD, Beard DJ, Kanis JA, Russell RGG. Intracellular inorganic-phosphate and ATP levels in human-blood erythrocytes, leukocytes and platelets in normal subjects and in diseases associated with altered phosphate-metabolism. Adv. Exp. Med. Biol. 1982; 151:147–155. [PubMed: 6295088]
52. Ryan LM, Rachow JW, McCarty BA, McCarty DJ. Adenosine triphosphate levels in human plasma. J. Rheu. 1996; 23:214–219.
53. Hoffman RM, Zhao M. Whole-body imaging of bacterial infection and antibiotic response. Nat. Protoc. 2006; 1:2988–2994. [PubMed: 17406559]
54. Mortin LI, Li T, Van Praagh ADG, Zhang S, Zhang X, Alder JD. Rapid bactericidal activity of daptomycin against methicillin-resistant and methicillin-susceptible staphylococcus aureus peritonitis in mice as measured with bioluminescent bacteria. Antimicrob. Agents Chemother. 2007; 51:1787–1794. [PubMed: 17307984]
55. Zhang H, Kalweri G, Mani N, Grossman TH. Development and validation of a multi-dose neutropenic rat thigh model using real-time monitoring of staphylococcus aureus growth in vivo. In Vivo. 2008; 22:667–672. [PubMed: 19180989]

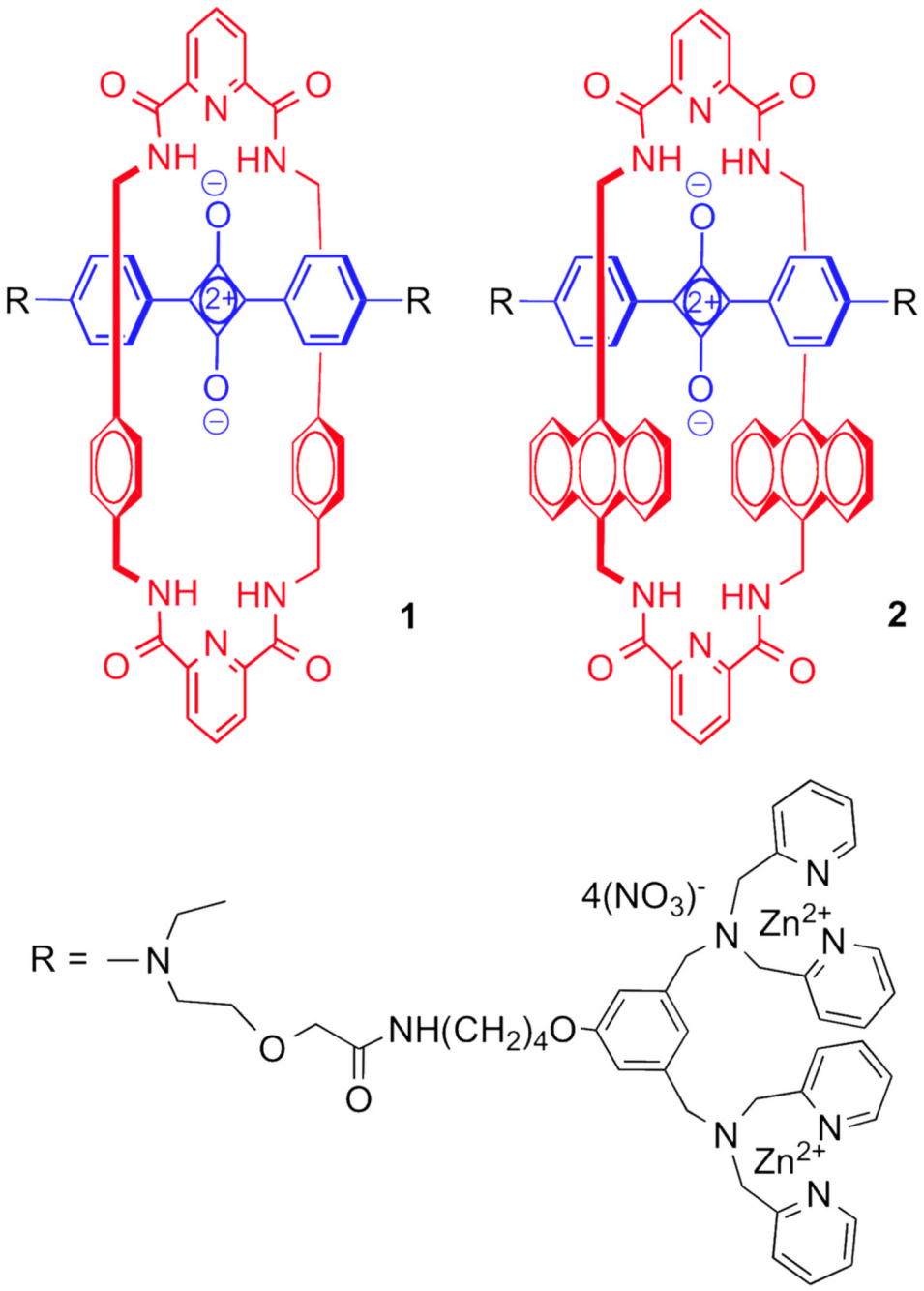

Figure 1.
Chemical structures of fluorescent probes.

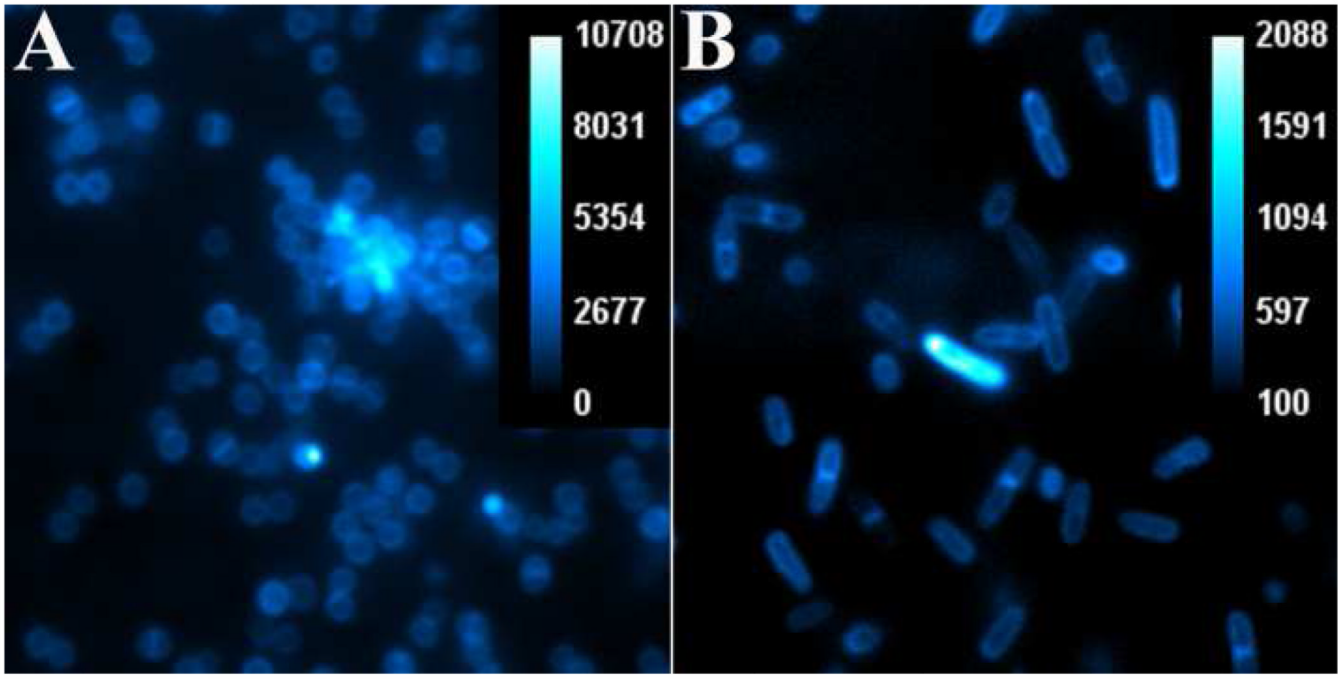

Figure 2.
Epifluorescence microscopy of planktonic *S. aureus* NRS11 (panel A) and *S. enterica* serovar typhimurium AM3 (panel B) after incubation of ~10^8 CFU with probe **1** (10 μM). Images viewed at 1500× magnification and show pixel intensity with scale bar in arbitrary units.

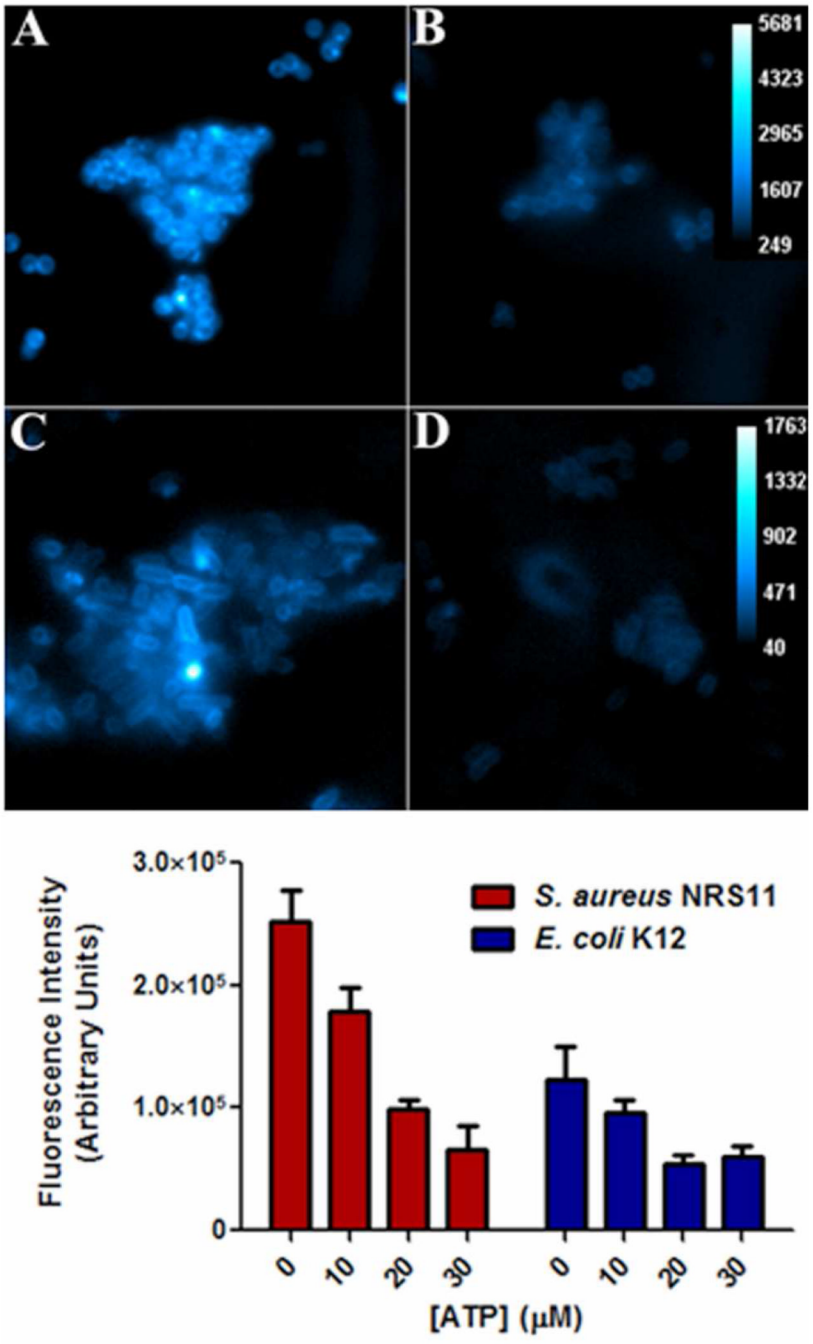

Figure 3.
(top) Fluorescence micrographs showing intensity of probe **1** (10 μM) staining of *S. aureus* NRS11 in the absence (panel A) and presence of 30 μM ATP (panel B), and intensity of *E. coli* K12 staining in the absence (panel C) and presence of 30 μM ATP (panel D). (bottom) Change in probe **1** staining intensity of bacteria as a function of added ATP.

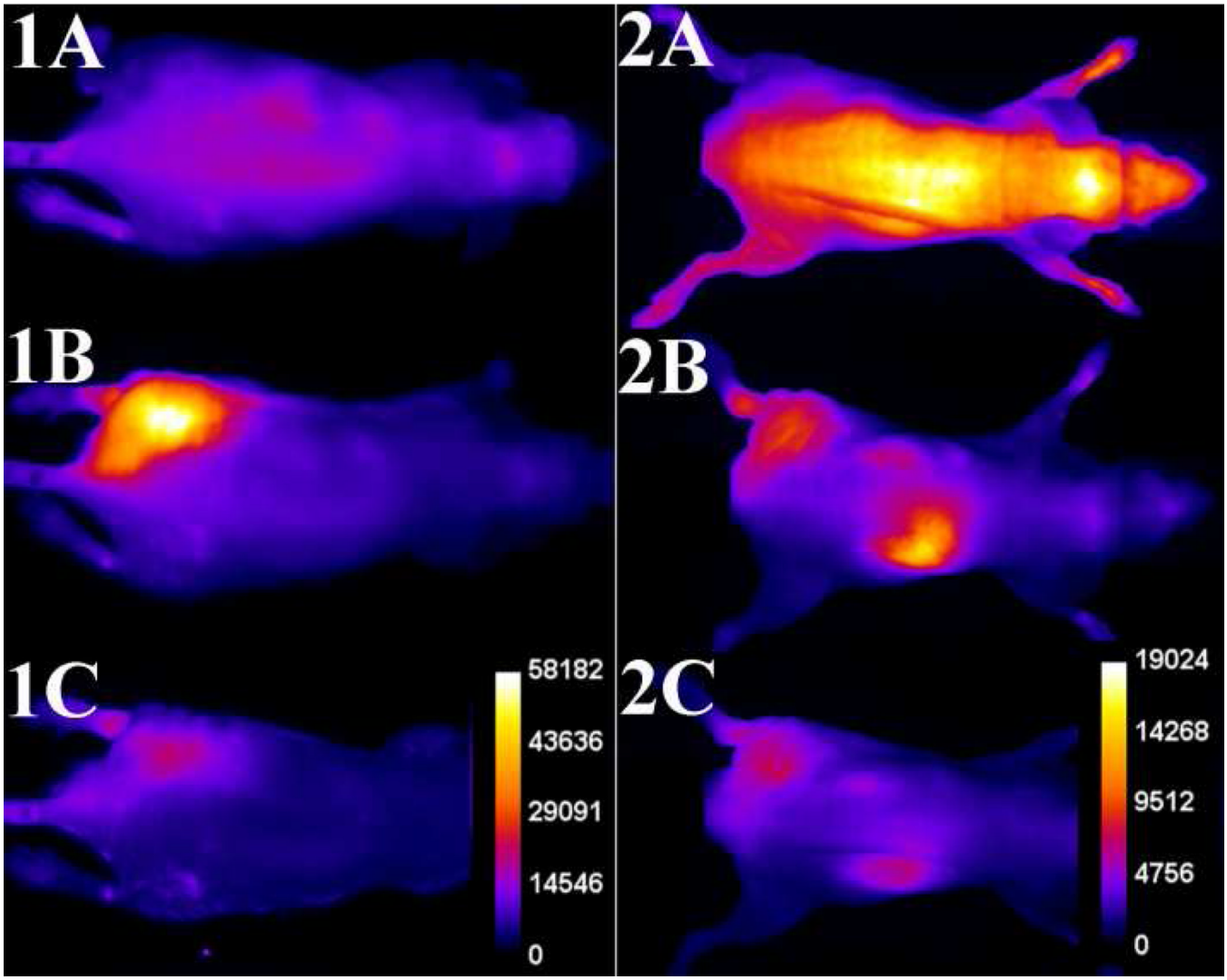

Figure 4.

Typical infection imaging montages. Nude, athymic mice were injected with *S. aureus* (~10^8 CFU) in LB broth (50 μL) in the left leg and sterile LB broth (50 μL) in the right leg. Six hours later, 10 nmol of probe **1** (series 1) or probe **2** (series 2) was injected via the tail vein, and whole-animal dorsal images were acquired at: [A] 0, [B] 3, and [C] 12 hours after probe dosage. The intensity scale bars (a.u.) apply to all images in each series.

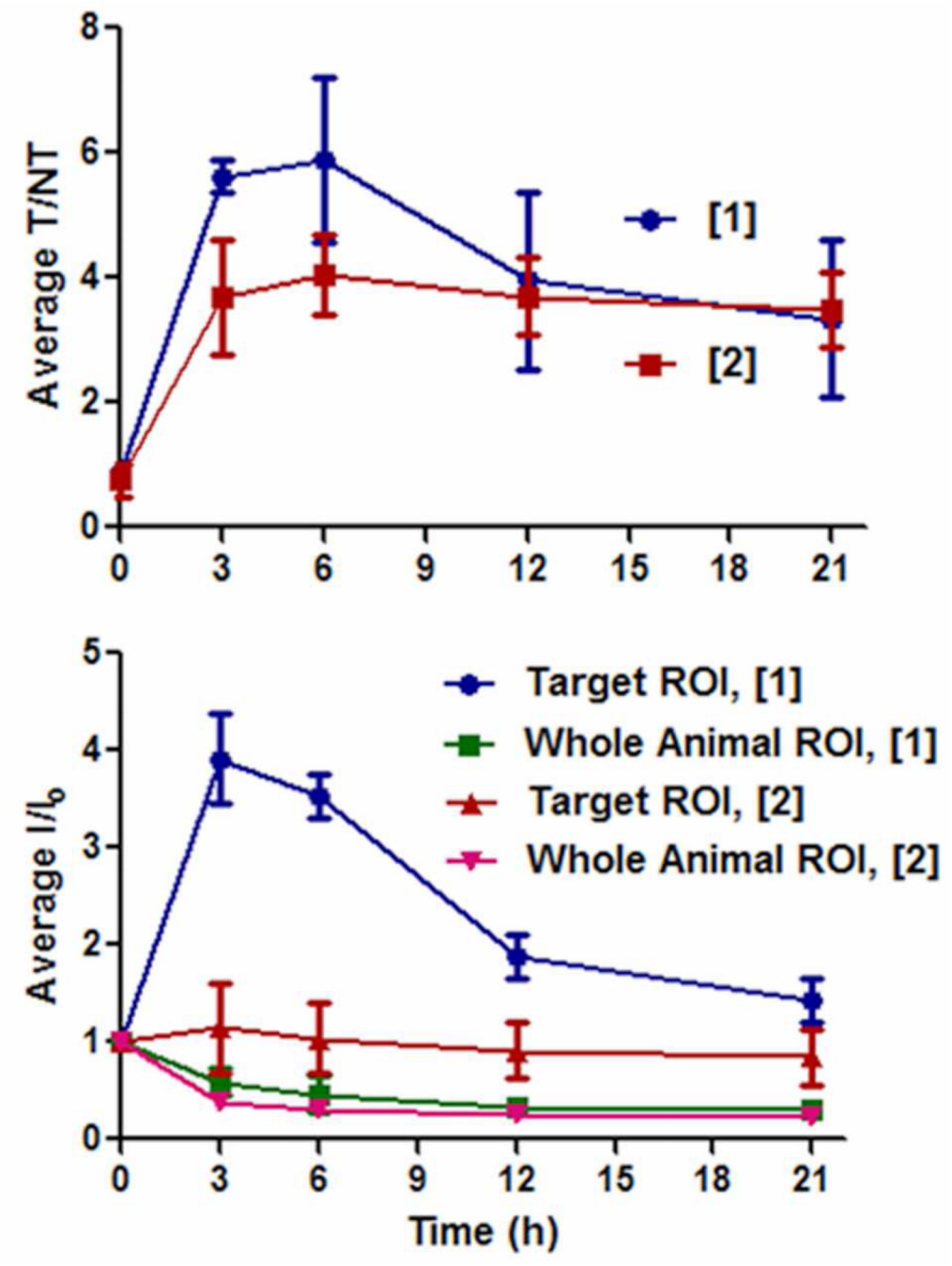

Figure 5.

Region-of-interest analysis of nude mouse infected with *S. aureus* and treated with probes **1** or **2**. (top) Ratio of signals for infected target leg (T) to uninfected non-target leg (NT). (bottom) Change in intensity for infected target leg and whole animal. Error bars reflect the standard error of the mean. N = 4 for probe **1**, N = 3 for probe **2**.

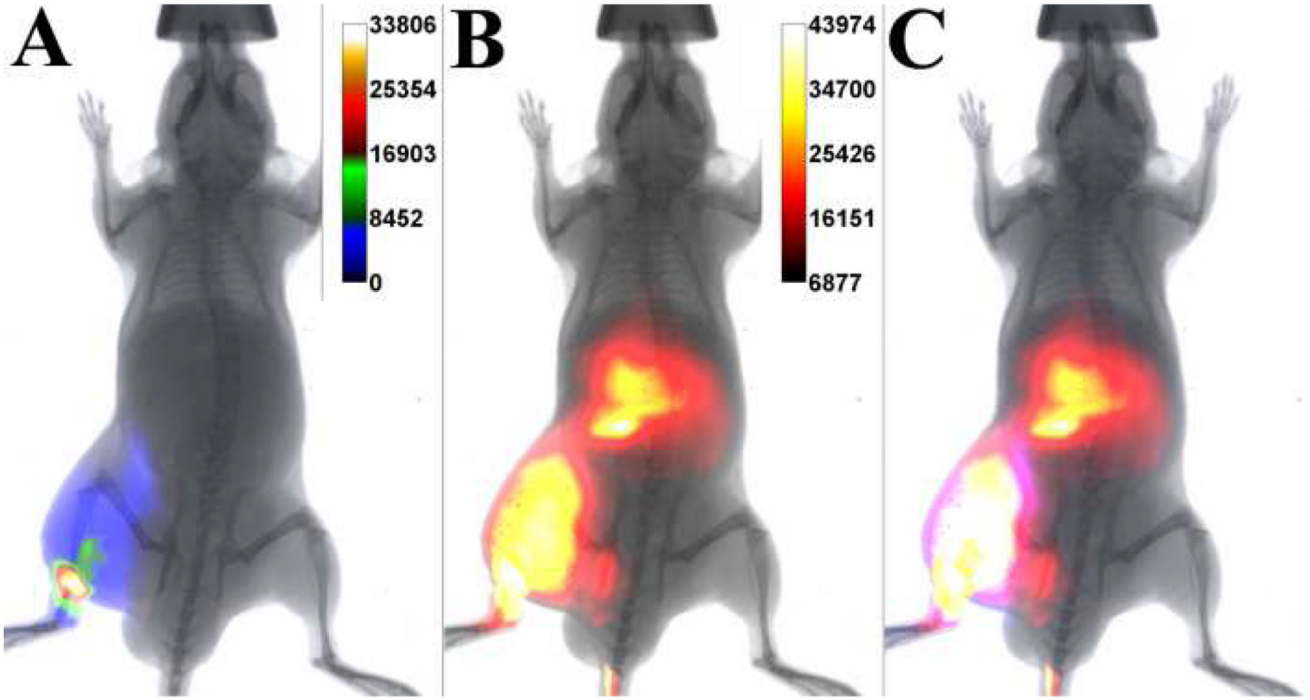

Figure 6.

Typical optical imaging of athymic mouse containing a Gram-negative bacterial infection. Overlaid ventral images of planar X-ray and; (A) bioluminescence intensity from genetically altered *S. enterica* serovar typhimurium FL6; (B) fluorescence intensity from molecular probe **1** at three hours after probe dosage; [C] bioluminescence and fluorescence intensities. N = 3.

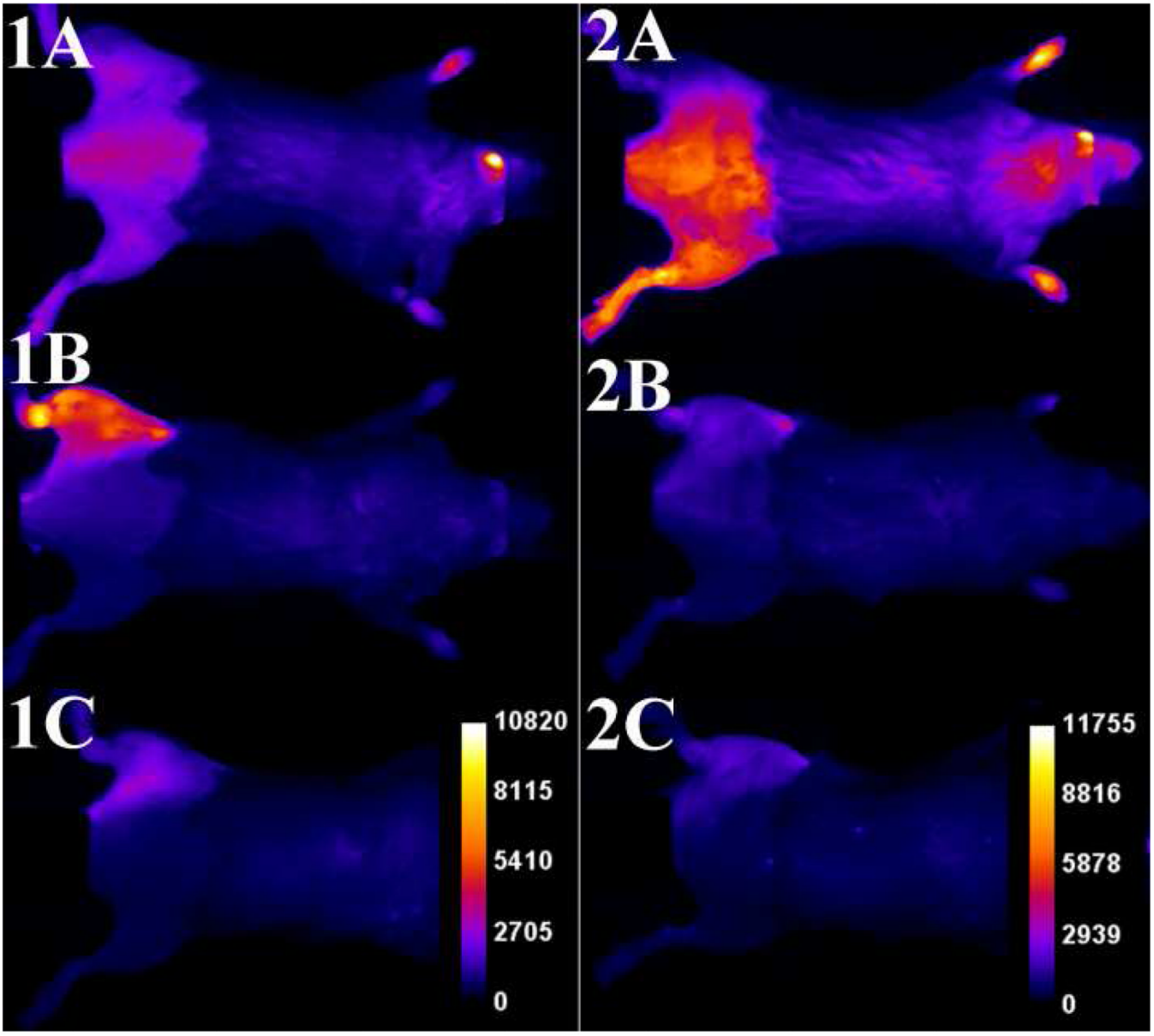

Figure 7.

Typical infection imaging montages. Immunocompetent mice were injected with *S. aureus* (~10^8 CFU) in LB broth (50 μL) in the left leg and sterile LB broth (50 μL) in the right leg. Six hours later, 10 nmol of probe **1** (series 1) or probe **2** (series 2) was injected via the tail vein, and whole-animal dorsal images were acquired at: [A] 0, [B] 3, and [C] 12 hours after probe dosage. The intensity scale bars (a.u.) apply to all images in each series. N = 3.

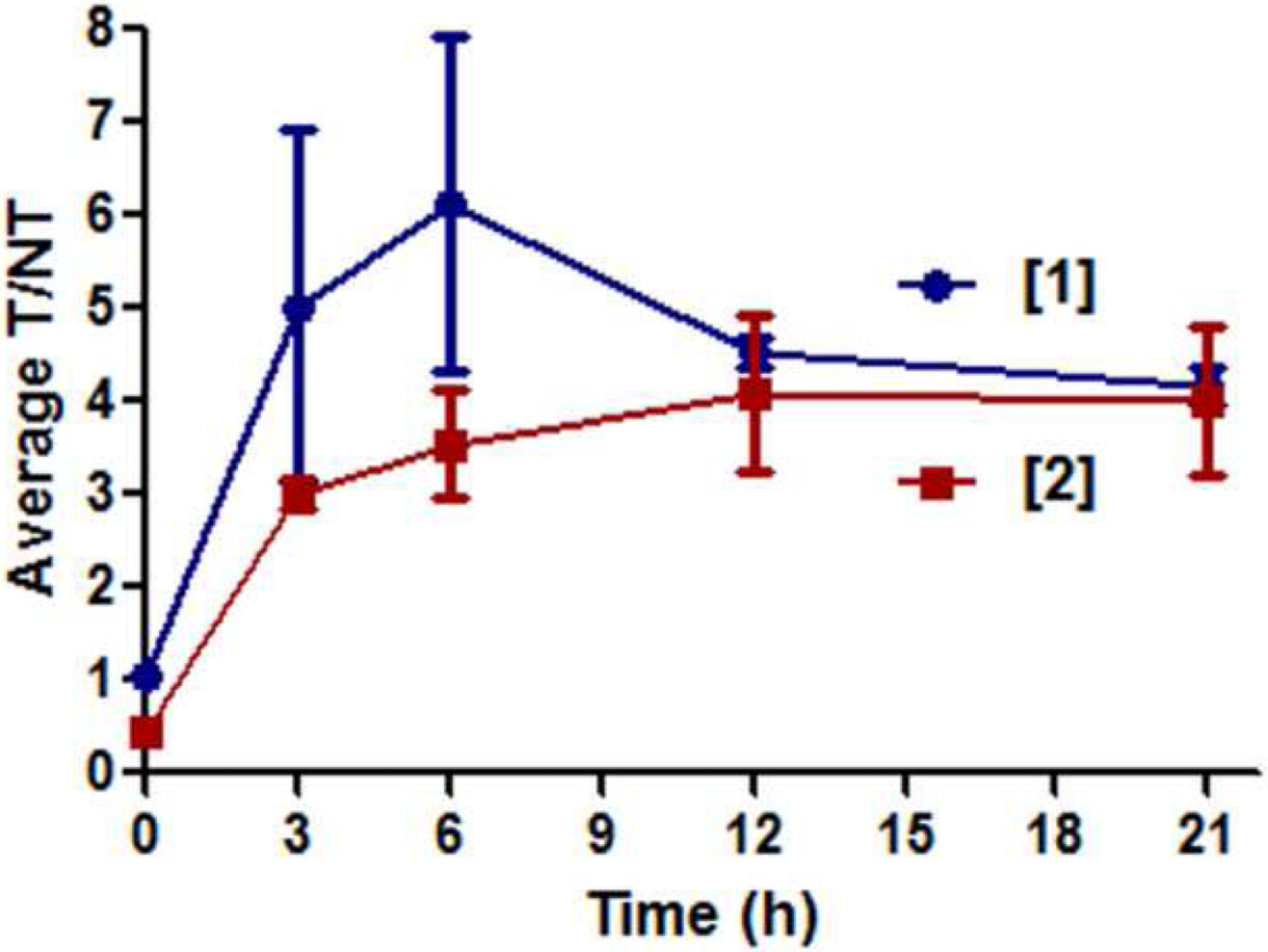

Figure 8.
Region-of-interest analysis of immunocompetent mice infected with *S. aureus* and treated with probes **1** or **2**. (left) Ratio of signals for infected target leg (T) to uninfected non-target leg (NT). Error bars are indicative of the standard error of the mean. N = 3 for both probes.

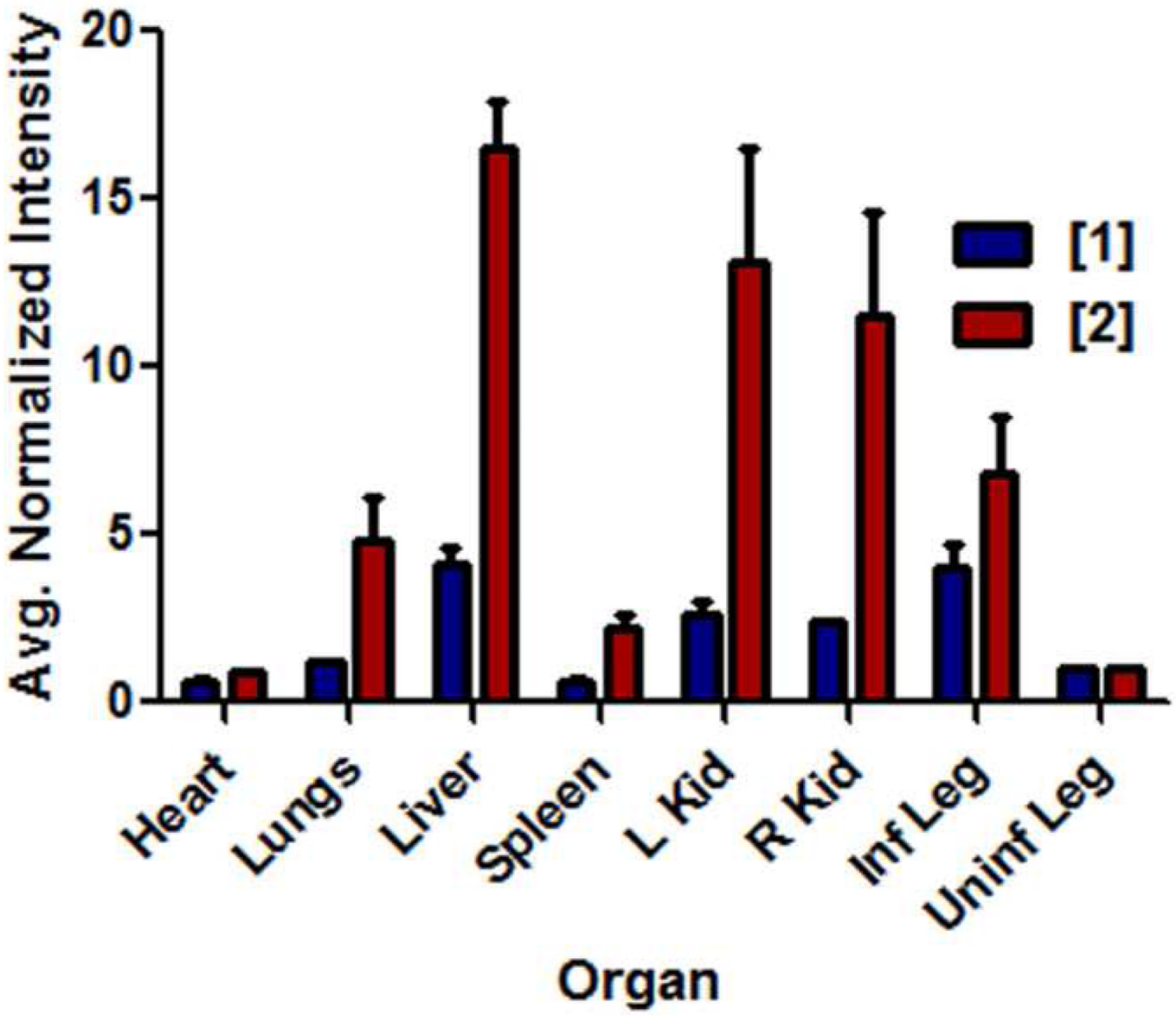

Figure 9.

Bar graph comparing the fluorescence of organs harvested from ICr mice that were infected in the left posterior leg with *S. aureus* NRS11 and treated with probe **1** or probe **2**. The animals were sacrificed at 21 h after probe dosage. All data is normalized to the fluorescence of the uninfected posterior leg in each animal. Error bars reflect the standard error of the mean. N = 3 for each group.

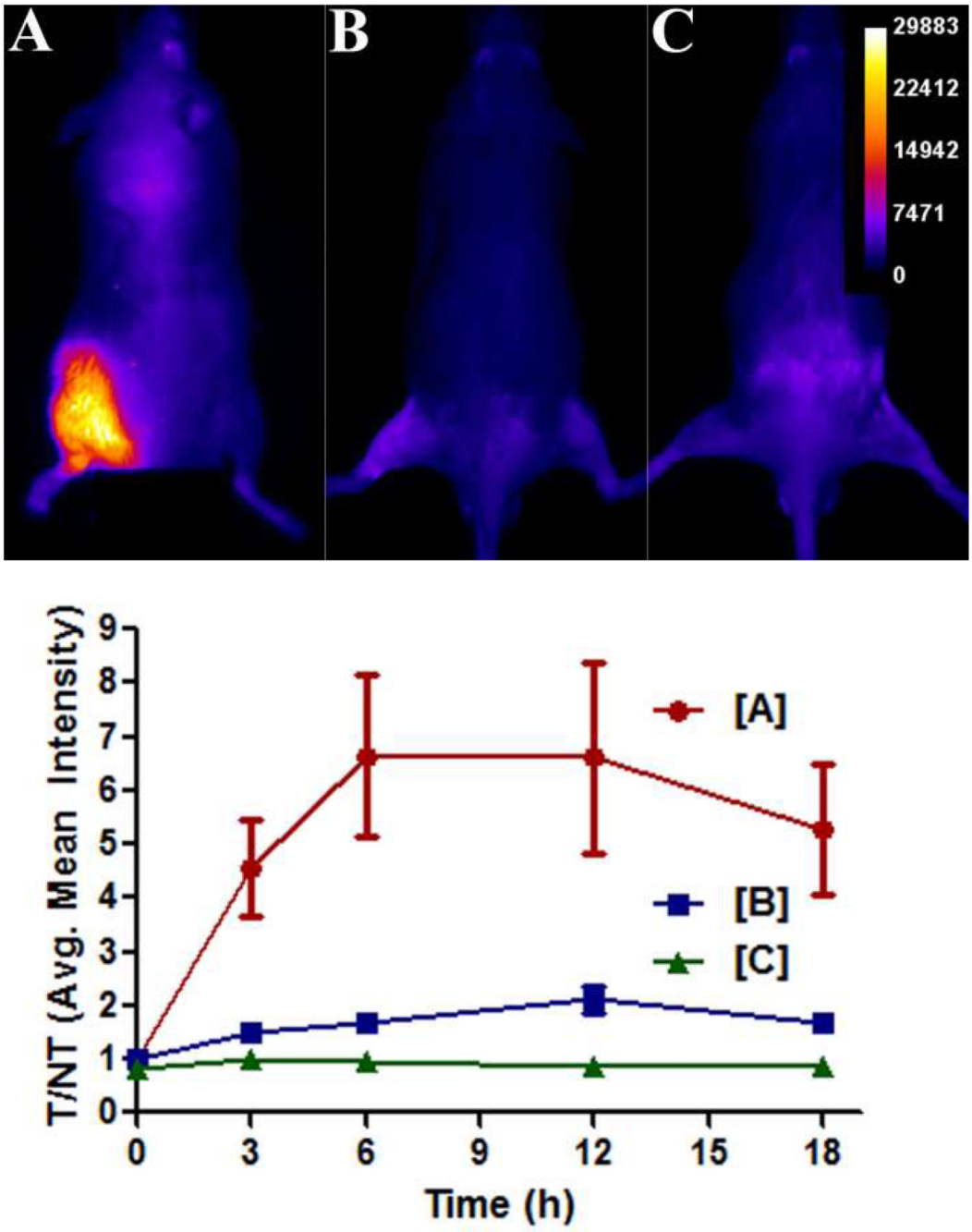

Figure 10.

Probe **1** targets bacterial infection and not sterile inflammation in immunocompetent mice (strain ICr). (top) Mice were treated with 10 nmol of probe **1** six hours after the left posterior leg was injected with ~10^8 CFU of *S. aureus* NRS11 [A], 50 μL of a 1 % λ-carrageenan solution [B], or 50 μL of a sterile saline solution [C]. The dorsal images were acquired at 12 hours post injection of probe. (bottom) Graph depicts the change in target-to-nontarget ratios (T/NT) obtained via ROI analyses of images. Error bars represent standard error of the mean. N = 3 for each group.